Annals of Biomedical Engineering, Vol. 30, pp. 537–545, 2002
Printed in the USA. All rights reserved.

0090-6964/2002/30(4)/537/9/$15.00

A Morphometric Model of Lung Mechanics for Time-Domain Analysis of Alveolar Pressures during Mechanical Ventilation

GIANLUCA NUCCI, SIMONLUCA TESSARIN, and CLAUDIO COBELLI

Dipartimento di Elettronica e Informatica, University of Padova, Italy

(Received 6 September 2000; accepted 25 February 2002)

Abstract—In this study we propose, and implement in the time domain, an anatomically consistent model of the respiratory system in critical care conditions that allows us to evaluate the impact of different ventilator strategies as well as of constrictive pathologies on the time course of acinar pressures and flows. We discuss the simplifications of the original Horsfield structure (Horsfield, K., *et al.* Models of the human bronchial tree. *J. Appl. Physiol*. 31:207–217, 1971), which were needed to enable the model implementation. The model has a binary tree structure including large airways represented as a combination of wall compliance and laminar resistance, small airways that have the same arrangement but can be heterogeneously constricted, and alveolar compartments that are viscoelastic second-order models to represent the stress adaptation behavior of lung tissue. We have described patient–ventilator interactions modeling the ventilator and the endotracheal tube. In conclusion this model makes it possible to investigate realistically the effect of homogeneous versus heterogeneous constrictive pathologies and the impact of different ventilatory patterns on pressure and flow distribution at the acinar level in the mechanically ventilated patient. © *2002 Biomedical Engineering Society.* [DOI: 10.1114/1.1475344]

Keywords—Lung mechanics, Artificial ventilation, Airways, Simulation model.

INTRODUCTION

Simulation models have been extensively used in breathing mechanics[5,10,11,14,24] and have favored the development of both new techniques for the assessment of respiratory mechanics at the bedside of the ventilated patient[1,15,25] as well as guidelines for optimizing ventilatory support.[6,19]

The most comprehensive and detailed models of breathing mechanics are those of Horsfield and co-workers,[12,13] which rely on morphometric measures. These models have often been employed to explain various facets of constrictive diseases.[7,8,17,18,28] All these studies have been performed in the frequency domain (FD) to reduce the computational burden of simulation. However, FD analysis has a number of shortcomings when simulating the respiratory system during artificial ventilation. First, the input impedance of all the respiratory mechanics models has a pole at zero frequency that prevents the evaluation of the mean pressure value. Therefore, using the FD approach; it is virtually impossible to correctly predict both peak and baseline pressure throughout airway and tissue structures. These quantities are important clinical indexes for the management of mechanically ventilated patients.[23] Second, FD analysis assumes that the system is in steady state, while the patient–ventilator coupling is a time-variant system. In fact, during inspiration the ventilator provides (at least to a certain amount) the pressure to inflate the patient's respiratory system. During passive expiration through the ventilator, the opposing pressure is augmented by the expiratory circuit, and therefore the switch from inspiration to expiration introduces a transient, time-variant response in the patient–ventilator system. Finally, since the resistance and compliance of the respiratory system are known to be volume and flow dependent,[20,22,26] FD analysis of such a large nonlinear system would be generally more demanding than a time-domain (TD) solution.

This scenario calls for a time-domain implementation of an anatomically consistent model of the respiratory system in critical care conditions which would allow the evaluation of different ventilator strategies as well as various bronchoconstriction levels on alveolar, or more correctly, on acinar pressures and flows. By starting from a FD implementation of the Horsfield structure,[7] we have developed a new TD simulation model of respiratory mechanics in ventilator-dependent patients. Some simplifications were needed in order to enable the numerical solution of the model, since a TD analysis of the complete Horsfield structure would require the solution of more than 60×10^6 differential equations. We propose a reasonable computational simplification that preserves anatomical fidelity. To do so we have taken advantage of the finite bandwidth of the waveforms used to ventilate the patients,[16] which excites the respiratory system over

Address correspondence to Professor Claudio Cobelli, Dipartimento di Elettronica e Informatica, Via Gradenigo 6/A, 35131 Padova, Italy. Electronic mail: cobelli@dei.unipd.it

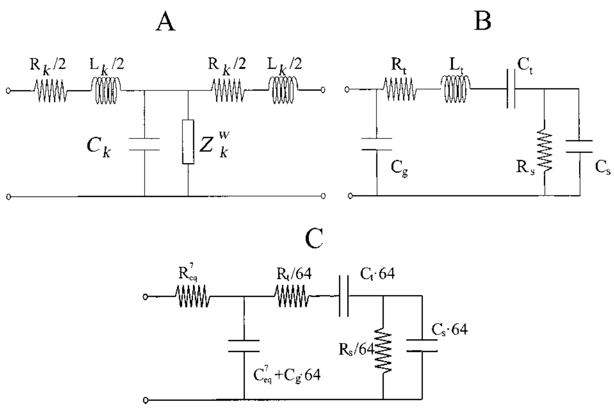

FIGURE 1. Panel (A): the acoustic transmission line for modeling the airway segment of order *k*. Panel (B): model of an alveolar–tissue unit. Panel (C): equivalent acinar structure composed of an equivalent resistance and a shunt compliance connected to an equivalent tissue model.

a limited frequency range (≤2 Hz), allowing for a reduction in the number of equations representing each airway. Moreover, we reduced the number of analyzed airways by modeling explicitely the conducting airways, while the pulmonary acini were lumped into equivalent airways leading to equivalent alveoli.

FREQUENCY DOMAIN MODEL

The model is a modification of a recently published[7] FD implementation of the asymmetric branching airway network of Horsfield *et al.*[12] The airway tree is classified by a dichotomously dividing system: each order has a specific length, diameter, and recursion index Δ. For order k, Δ_k identifies the order of the two descending daughters at each bifurcation. Additional morphometric data include the thickness and amount of cartilaginous relative to soft tissue (ca_k) of the airway wall.[9]

By modeling each airway as a rigid tube, it is possible to model a single segment of the Horsfield airway tree with a lumped parameter description[2] with further simplifications assuming low frequencies (<10 Hz) excitation.[28] The mechanics of the airway wall can be modeled with tissue with tissue resistance–inertance–compliance in parallel with gas compression compliance.[27] Hence, each segment of the airway tree can be represented with the acoustic transmission line of Fig. 1(A).

The terminal airways lead to a tissue element consisting of a shunt gas compression compliance for the alveolus and a viscoelastic tissue model [Fig. 1(B)] to account for the stress adaptation of the lung parenchyma. Each alveolus has an impedance that is equivalent to the total pulmonary impedance divided by the number of alveoli. The following parameter values, for the normal lung, were used in the simulations.[3] $R_t = 0.4$ cm H_2O s/l, $C_t = 0.122$ l/cm H_2O, $R_s = 3.4$ cm H_2O s/l, $C_s = 0.3125$ l/cm H_2O, where R_t is the viscous component of lung tissue resistance, C_t the static compliance, and R_s, C_s the Maxwell body accounting for the viscoelastic behavior of the lung.

The equivalent input impedance of the model can be computed in the FD by recursively calculating the impedance of each airway and by combining the impedances in the appropriate serial and parallel association.[9,18] Heterogeneous airway constriction can be modeled by a Gaussian distribution.[18,28] Thus, the constricted radius (r^c) is obtained from the baseline one (r) according to

$$r_k^c = r_k(1 - \mu/100)(1 + nCV/100), \tag{1}$$

where k is airway order, n is a random number sampled from a normal distribution (with mean 0 and variance 1), μ ($0 \leqslant \mu < 100$) is the percent constriction level, and CV ($0 \leqslant \mathrm{CV} < 100$) is the percent coefficient of variation.

TIME-DOMAIN MODEL

The time-domain implementation of the Horsfield model was encoded using the circuit simulation software SPICE.[29] Moving from FD to TD analysis is, in principle, simple. However, while in the frequency domain the model equations can be simplified by algebraic manipulation, a TD solution cannot resort to symbolic calculus. So, with the Horsfield model, one has to face the solution of about 60×10^6 differential equations, seven for each airway segment [Fig. 1(A)] and four for each alveolar compartment [Fig. 1(B)], which constitutes a prohibitive computational burden. Consequently, there is the need to find a trade off solution which, while maintaining an anatomically detailed structure, allows us to arrive at a workable model. The overall strategy aimed at simplifying the model structure implemented in the FD by Gillis and Lutchen.[7] To do so we took advantage of the limited bandwidth of the signals commonly adopted in the intensive care unit (ICU) to ventilate the patients that display 98% of their spectral energy in the 0–2 Hz range.[16] This justifies a first simplification of the airway and of the alveoli structures, by only including in the analysis the influence of airway inertance for the larger airways (> of order 29). In addition, in the low-frequency range, airway wall resistance and inertance are assumed to be negligible.[21] Thus, in principal, airway gas compressibility and wall compliance can be lumped together into a single parallel compliance. The number of components in the model can also be reduced by lumping the two $R_k/2$ resistance of Fig. 1(A) into a single R_k resistance shunted by the parallel gas–wall compliance. Hence, the tissue elements can also be simplified by considering the airway and the alveolar shunt gas com-

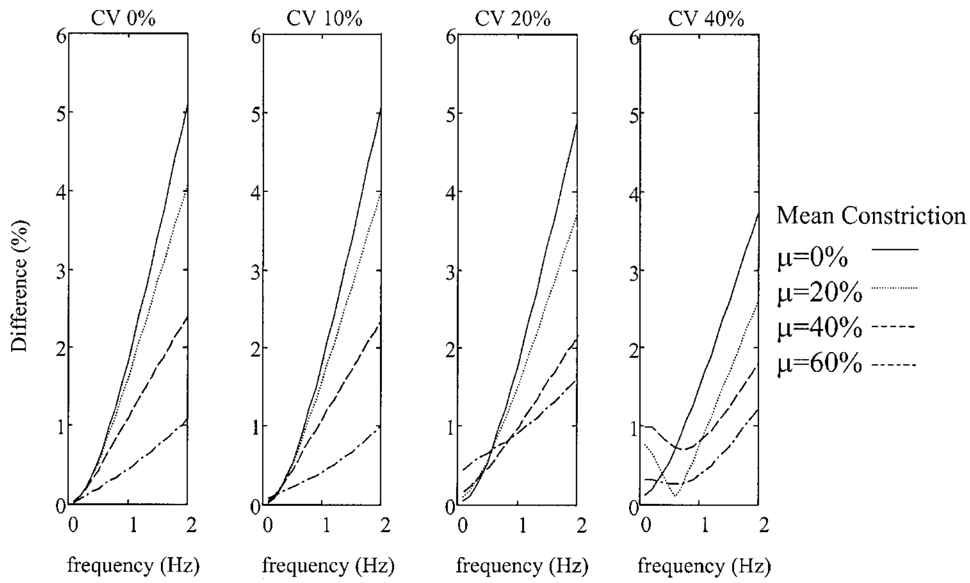

FIGURE 2. Absolute value of the percentage difference between the input impedance of the Horsfield model and that of the simplified one. Different mean constriction (μ) and heterogeneity (CV) levels are shown. Increasing levels of heterogeneity are displayed, from left to right, from homogeneous (CV=0%) to highly heterogeneous (CV=40%). For each panel four mean constriction levels are shown: μ=0% (solid), 20% (dotted), 40% (dashed), and 60% (dash dot).

pression compliance in parallel. All these simplifications have little effects on the input impedance spectrum out to 2 Hz. In fact, Fig. 2 shows the absolute value of the difference (in percent) between the input impedance of the Horsfield structure (Z_I) and the simplified one (Z_I^s) for different airway constriction ($0 \leqslant \mu \leqslant 60$) and heterogeneity ($0 \leqslant \mathrm{CV} \leqslant 40$), calculated as

$$\mathrm{Difference} = \frac{100|Z_I(f) - Z_I^s(f)|}{|Z_I(f)|}, \tag{2}$$

where f is frequency ($0 \leqslant f \leqslant 2$ Hz). However, albeit the number of differential equations is now reduced to $\cong 13 \times 10^6$, the model dimension is still excessive by a large amount for a TD solution.

The next step was the simplification of the terminal structure of the airway tree (where the number of elements rises exponentially). To do so we decided to explicitly model the conducting airways (from order 35 to order 8) and to lump the impedance of the acinar airways (order 7–1) into a single equivalent terminal bronchiole composed by a resistance and a shunt compliance. The equivalent airway is connected to an equivalent alveolus representing the load of 64 parallel alveolar–tissue elements [see Fig. 1(C)]. To calculate the acinar parameters and allow for constriction in the terminal Horsfield structure we have exploited the equations characterizing the acoustic transmission line under order 7:

$$R_k = \frac{8\eta l_k}{\pi r_k^4}, \tag{3}$$

$$C_k^g = \frac{\pi l_k r_k^2}{P_0}, \tag{4}$$

$$C_k^w = \frac{2\pi l_k r_k^3}{Y h_k}, \tag{5}$$

$$h_k = \sqrt{r_k^2 + \frac{\mathrm{WA}_k}{\pi}} - r_k, \tag{6}$$

where k is the airway order; R_k, C_k^g, and C_k^w are the airway resistance, gas compressibility compliance, and airway wall compliance, respectively; WA_k is the wall area; and h_k is the thickness of the airway wall. l_k and r_k are the length and radius of the airway segment, η is the air viscosity, ρ is the gas density, P_0 is the fixed pressure, and Y is the Young modulus associated with soft tissue.

Dealing with the equivalent acinar airway one can omit the subscript k. If μ is the homogeneous constriction level applied to the airway, we then have a change in the airway radius, which becomes $(1-\mu/100)r$. In order to find an equivalent resistance and compliance for the acinar airways we have calculated the spectrum of the subnetwork from order 7 to alveoli for various homogeneous constriction levels (0%–60%). These data

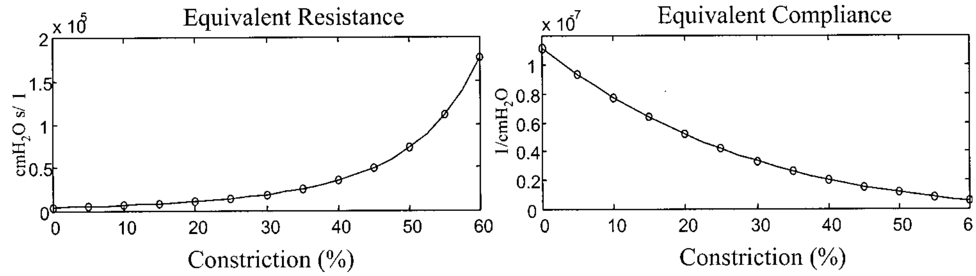

FIGURE 3. Equivalent resistance (left) and compliance (right) as a function of homogeneous constriction. Open circles are the equivalents calculated with the complete structure, solid lines are the least-squares fit obtained from Eqs. (7) and (8).

were fitted to the frequency response of the circuit of Fig. 1(C). In this way we obtained the values of the equivalents (open circles in Fig. 3) for different μ levels.

Letting $x=(100-\mu)$, and collecting all the constants and parameters not dependent on constriction, one has

$$R_{\mathrm{eq}}=\frac{8\,\eta l}{\pi r^4 x^4}=\frac{\alpha_1 A_1}{x^4}. \tag{7}$$

Remembering that for the simplified airway C_k^g and C_k^w are parallel compliances, by substituting Eq. (6) in Eq. (5) one has

$$C_{\mathrm{eq}}=C^g+C^w=\frac{\pi l r^2 x^2}{P_0}+\frac{2\cdot\pi\cdot l\cdot r^3\cdot x^3}{Y\left(\sqrt{r^2\cdot x^2+\dfrac{\mathrm{WA}}{\pi}}-r\right)}$$

$$=\alpha_2 A_2 x^2+\frac{\alpha_3 A_2 x^3}{\sqrt{x^2+A_3}-x}, \tag{8}$$

where α_1, α_2, and α_3 are constants and A_1, A_2, and A_3 are parameters to be estimated by fitting Eqs. (7) and (8) to the data of Fig. 3:

$$A_1=\frac{l}{r^4}, \tag{9}$$

$$A_2=lr^2, \tag{10}$$

$$A_3=\frac{\mathrm{WA}}{r^2}. \tag{11}$$

Equations (7) and (8) provided an excellent nonlinear least-squares fit (solid lines in Fig. 3) to the calculated equivalent resistance and compliance and, in addition, from the parameter estimates values one can derive length, diameter, and wall area of the equivalent acinar airway (which can thus be bronchoconstricted to a randomly selected level). In this way one loses information regarding the flow and pressure distribution in the respiratory airways but still obtains a reasonable approximation to the mechanical behavior of the equivalent acinar resistance and compliance under different conditions of bronchoconstriction (Fig. 3).

The above simplification assumes that the alveolar ducts of an individual acinus all undergo the same degree of bronchoconstriction. Thus, the TD implementation of the model does not allow for the same degree of heterogeneity as the FD implementation. Figure 4 reports the FD differences, calculated according to Eq. (2), between the complete and the simplified structure at different levels of heterogeneity and bronchoconstriction.

With the above simplifications one has a system of ≅210,000 differential equations that are solvable in the TD. It was also possible to include in the TD simulation model the effect of the chest wall impedance both at the tissue and at the intrathoracic airway level, as shown in Fig. 5. Note that gas compressibility at the alveolar level is referred to atmospheric pressure while airway wall compliance is referred to pleural pressure. This choice is physiologically sound but raises the dimension of the system to 270,000 differential equations. We, therefore, decided to split the influence of gas vs. wall compliance only at the acinar/alveolar level (where gas compression plays an important role) while leaving all the intrathoracic airways with a single compliance connected to pleural pressure. The chest wall load was described with a second-order viscoelastic tissue model using the parameter values reported by D'Angelo *et al.*[3]

The patient–ventilator coupling has been described so as to mimic typical ICU-like conditions. Generation 35 of the model has been bypassed by an endotracheal tube (ET) modeled according to Rohrer's equation:

$$R_{\mathrm{ET}}=K_1+K_2|\dot{V}|, \tag{12}$$

where the values of K_1 and K_2 were chosen from previously published data.[4] Inspiratory flow is provided to the lung model by a waveform generator, while the synchronizer switches, at prefixed times, between inspiration

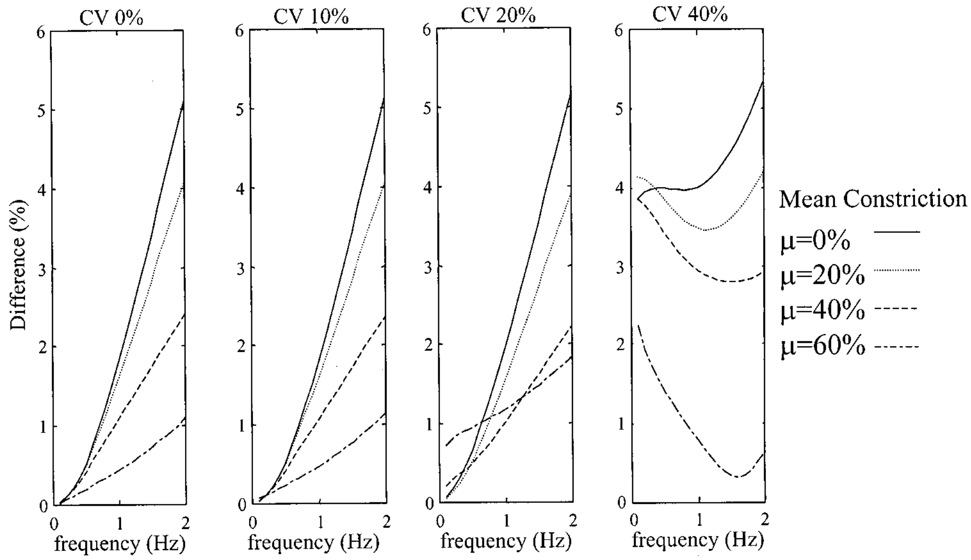

FIGURE 4. Absolute value of the difference (in percent) between the input impedance of the complete Horsfield structure and the TD model. Different mean constriction (μ) and heterogeneity (CV) levels are shown. Increasing heterogeneity levels are represented from left to right panels.

and expiration (which is passive). The expiratory circuit impedance is modeled as a nonlinear Rohrer resistance.[4] In this work we will focus only on airway opening and acinar signals, however, pressure and flow are accessible in all nodes of the Horsfield model.

SIMULATION

To analyze the effect of different constriction patterns on the distribution of alveolar pressures and flows during mechanical ventilation (MV) we simulated constant flow ventilation with a delivered tidal volume (V_T) of 0.6 l (8.57 ml/kg for a 70 Kg subject), an inspiratory time of 0.8 s, an end inspiratory pause of 0.4 s, and expiratory time of 2.8 s (corresponding to a breathing rate of 15 breaths/min).

We have simulated the following patient conditions:

- baseline, i.e., no constriction ($\mu = 0\%$) and no heterogeneity (CV=0%);
- medium constriction ($\mu = 40\%$) and medium heterogeneity (CV=20%);
- high constriction ($\mu = 60\%$) and low heterogeneity (CV=10%);
- moderate constriction ($\mu = 20\%$) and high heterogeneity (CV=40%).

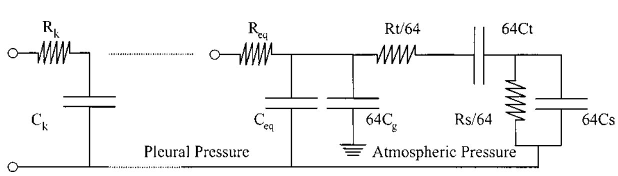

FIGURE 5. Scheme showing the pressure links of the TD model. Note that all the intrathoracic airways are connected to pleural pressure, while alveolar gas compressibility is connected to atmospheric pressure.

For each of the four simulations airway opening pressure (P_{ao}), flow ($\dot{V}$), tracheal pressure (P_{tr}), pleural pressure (P_{pl}), and a large sample of acinar pressures and flows ($P_{aci}, \dot{V}_{aci}$) were recorded. Simulations were carried out with SPICE,[29] which solves the model differential equations by employing a variable order trapezoidal method with a relative tolerance error of 0.1%. Data were simulated at 20 Hz sampling frequency. The respiratory cycles were analyzed after 20–40 breaths, i.e., after all the pressures in the airway tree have reached a periodic steady state. To achieve a faster integration convergence we employed a closure threshold rule that resulted in a complete closure of any airway constricted more than 90% of its baseline diameter.

Figure 6 shows the predicted input/output (I/O) signals (mouth flow and tracheal pressure) for the various constriction patterns. Figures 7–9 show the cumulative distributions of normalized acinar tidal volumes, baseline pressures, and peak alveolar pressures. We derived these distributions from the analysis of a large sample of simulated $\dot{V}_{aci}$ and P_{aci}. In order to have a reliable picture of pressure and flow distributions we have saved and processed traces until the resulting distribution was not significantly different from the previous one. Therefore, the sample size used varied from 200 in the homogeneous, to 2000 in the extremely heterogeneous case.

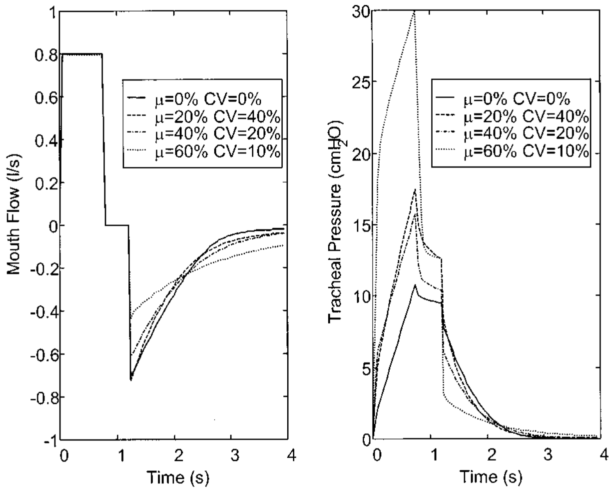

FIGURE 6. Simulated mouth flow (left panel) and tracheal pressure (right panel) for different constriction and heterogeneity levels: baseline (solid), moderate constriction with high heterogeneity (dashed), medium constriction with medium heterogeneity (dash-dot), and high constriction with low heterogeneity (dotted).

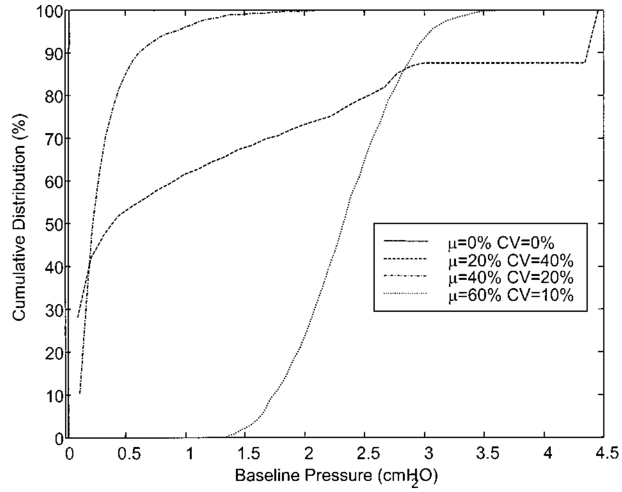

FIGURE 8. Cumulative distributions of baseline pressure at the acinar level. The four conditions shown correspond to the constriction patterns of Fig. 6.

RESULTS AND DISCUSSION

Model Development

The FD comparison between the complete and simplified models (Fig. 4) shows that our time-domain simulation model reproduces with reasonable accuracy (≅95%) the impedance spectra of the model proposed by Gillis and Lutchen[7] over a bandwidth that encompasses the spectral content of the commonly adopted ventilator waveforms. This is particularly true if one matches the results of Figs. 4 and 2, where the differences are due not to a structure reduction (number of terminal airways) but to a component simplification. It is worth noting that for each constriction level and for low–medium heterogeneity, the greater differences are found at higher frequencies (due to the inertance simplification) where the frequency content of the flow signal is small and thus there is little contribution to the overall response of the system. For a highly heterogeneous lung the error increases at low frequency (2%–4%) due the simplifying hypothesis that all the airways pertaining to a certain acinus behave symmetrically. However, the normalized difference error remains acceptable (around 5%).

The domain of validity of the mathematical model is necessarily limited. First, we modeled the airway tree with linear elements to make our simulations more manageable, even if both during spontaneous breathing and

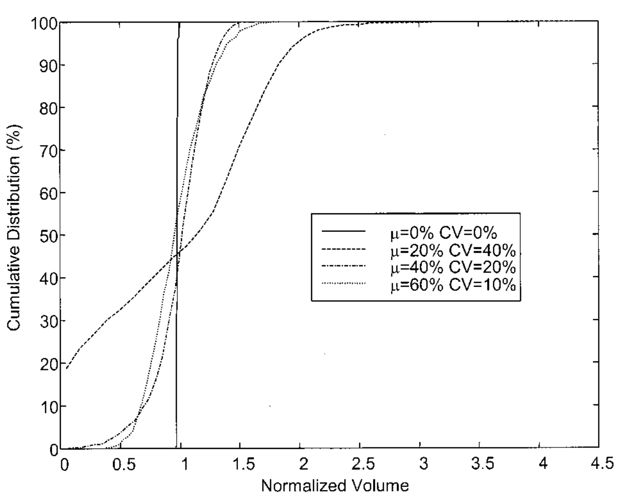

FIGURE 7. Cumulative distributions of the normalized acinar tidal volumes. The four conditions shown correspond to the constriction patterns of Fig. 6.

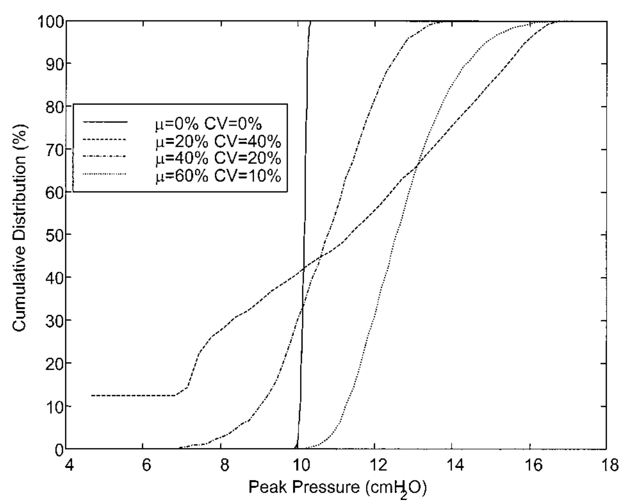

FIGURE 9. Cumulative distributions of peak pressure at the acinar level. The four conditions shown correspond to the same constriction patterns of Fig. 6.

mechanical ventilation this hypothesis is not true. Second, we did not include in our model the distensibility of the breathing circuit. This was done to make sure that the delivered V_T in the four simulated cases were equal (the flow delivered by the ventilator would partition between the patient and the tube compression compliance).

Input/Output Behavior

The TD anatomically consistent model allowed us to simulate the time course of the I/O signals (Fig. 6) and acinar dynamics during MV with different constriction and heterogeneity levels. Figure 6 shows how the viscoelastic properties of the respiratory system modulate the rate of passive expiration. The different expiratory flow patterns can be explained in the light of a first-order model of respiratory mechanics that, even if simplistic, predicts the expiratory flow according to the formula

$$\dot{V}_e = -\frac{V_T}{\tau} e^{-t/\tau}, \tag{13}$$

where τ is the respiratory system time constant, i.e., total resistance over total elastance (R_T/E_T). In the four cases analyzed, in line with the results of Lutchen and Gillis,[18] we have different respiratory system mechanics. A fairly homogeneous constriction results in a marked increase in R_T at the breathing frequencies with E_T only slightly augmented (this results in an increased τ). In contrast, during highly heterogeneous constriction, both R_T and E_T are much higher than the baseline, due to airway closure, thus resulting in a τ value similar to the normal case.

Comparison of the tracheal pressure traces confirms that constriction induces a marked increase in the total load of the respiratory system. Note that the total pressure response to the square flow wave in the $\mu = 20\%$, $\mathrm{CV} = 40\%$ case is higher than in the $\mu = 40\%$, $\mathrm{CV} = 20\%$ one, indicating, in line with previous FD models, that heterogeneity amplifies the effects of constriction.[17,18,28]

Acinar/Alveolar Behavior

How does this I/O behavior reflect at the acinar level? Figure 7 shows the cumulative distribution of acinar V_T normalized by the number of acini and the mouth V_T (for a homogeneous, symmetrical, and rigid model one should expect a vertical line centered in 1). In fact, the baseline simulation yields a very narrow distribution with all the acini lying in the 0.965–1.003 interval. Medium constriction and heterogeneity (dash-dot line) yields a markedly broader volume distribution (ranging from 0.06 to 1.5); however, 80% of the acini is still distributed in a ±30% range of the baseline volume, thus overdistension appears unlikely. This is found also in the $\mu = 60\%$, $\mathrm{CV} = 10\%$ case (dotted line). All the acinar V_T are in the 0.4–1.8 range (thus moved to higher volumes), but again, looking at the central 80% of acini, we have that they lay in the 0.7–1.3 range. This shows how constriction *per se* amplifies the effect of heterogeneity on volume distribution at the acinar level given that the $\mu = 40\%$, $\mathrm{CV} = 20\%$ and $\mu = 60\%$, $\mathrm{CV} = 10\%$ cases yield pretty similar distributions. Increasing the level of heterogeneity and allowing some airways to close, e.g., like in the highly heterogeneous constriction ($\mu = 20\%$, $\mathrm{CV} = 40\%$), leads to dramatic changes in the volume distribution with 20% of acinar units receiving less than 10% of the baseline volume (12.5% were nonventilated) and 30% receiving at least 50% more volume than in the healthy case (this results in an increased risk of volutrauma at each ventilator cycle).

Baseline pressure distributions (Fig. 8) are a measure of dynamic PEEP_i[23] [i.e., the raise of end expiratory pressure above functional residual capacity (FRC)] due to changes in respiratory mechanics. In fact, with the simulated ventilator settings (low V_T and extended expiratory time) we have very low baseline pressures (0.02–0.03 cm H_2O) in the unconstricted case. The $\mu = 40\%$, $\mathrm{CV} = 20\%$ simulation yields an increase in baseline pressure with 80% acini in the range 0.2–0.62 cm H_2O with highest values of about 2 cm H_2O. The high-constriction–low-heterogeneity case displays a baseline pressure distribution that is shifted towards higher values ranging from 1.3 to 3.75 cm H_2O (80% of acini are in the 1.75–2.92 cm H_2O order) due to the remarkable decrease in the respiratory system time constant. Heterogeneous constriction affects markedly the baseline pressure distribution, yielding a consistent portion (30%) of healthy units whose dynamic PEEP_i is lower than 0.12 cm H_2O, together with 20% of the units displaying a baseline pressure level higher than 2.55 cm H_2O. Note that the more hyperinflated acinar units are those connected to a high impedance airway path (thus receiving a low volume) and that the nonventilated acini have a pressure trace that is constant and equal to the mean acinar pressure (4.45 cm H_2O in this case). Indeed, by looking at the peak pressure distributions (Fig. 9) one observes that 30% of peak acinar pressure in the $\mu = 20\%$, $\mathrm{CV} = 40\%$ case are lower than 8.31 cm H_2O, while the peak pressure of the healthy case are distributed between 9.9 and 10.35 cm H_2O. Moreover, we found that in the highly heterogeneous case, 15% of respiratory units receive a peak pressure 50% higher than the $\mu = 0\%$, $\mathrm{CV} = 0\%$ case (suggesting an increased risk of barotrauma). The $\mu = 60\%$, $\mathrm{CV} = 10\%$ constriction pattern produced a significant increase in the peak pressure in all the acini (80% acini are in the range 11.26–14.37 cm H_2O), but our simulations indicate that only 3% of the units are receiving a peak pressure 50% higher than baseline.

Note that all the stochastic distributions of Figs. 7–9 are non-Gaussian, albeit have been generated from Gaussian constriction patterns: in fact, flow/pressure distributions depend from the airways impedance arrangement that is a complex nonlinear function of the normally distributed radii. Moreover, in the severely heterogeneous constriction there is a consistent number of nonventilated acini, all behaving symmetrically, that add further nonlinearities in the distributions.

In conclusion, we have developed an anatomically based model to quantitatively analyze flow and pressure alveolar dynamics in mechanically ventilated patients. The TD approach was a necessity to obtain acinar pressure distribution and to account for the time variance of the mechanical ventilator–patient interaction. The TD implementation of the Horsfield structure required a careful simplification in order to find a suitable compromise between including in the model as much anatomical details as possible and allowing a feasible computer implementation. This solution enabled us to perform simulations of conventional mechanical ventilation, and thus to evaluate the impact of different constriction patterns on the flow/pressure distributions at the acinar level. We found that heterogeneity of bronchoconstriction rather than mean constriction level, plays a major role in determining the impairment of pressure and volume distribution at the acinar level. In addition, a severe heterogeneous constriction can markedly increase the risk of ventilator-induced lung injuries (barotrauma–volutrauma).

Thus, this anatomically detailed model candidates as a reliable tool to analyze flow and pressure distribution in the airway tree both in spontaneous breathing and in mechanical ventilation.

ACKNOWLEDGMENTS

This work was supported in part by a grant from the Italian Ministero dell'Università e della Ricerca Scientifica e Tecnologica (Bioingegneria del Sistema Respiratorio). The authors thank Professor K. R. Lutchen for having provided the code of the frequency domain simulation model. The authors are grateful to the reviewers for their helpful comments.

REFERENCES

[1] Bates, J. H. T., P. Baconnier, and J. Milic-Emili. A theoretical analysis of interrupter technique for measuring respiratory mechanics. *J. Appl. Physiol.* 64:2204–2214, 1988.

[2] Benade, A. H. On the propagation of sound waves in a cylindrical conduit. *J. Acoust. Soc. Am.* 26:726–731, 1968.

[3] D'Angelo, E., F. M. Robatto, E. Calderini, M. Tavola, D. Bono, G. Torri, and J. Milic-Emili. Pulmonary and chest wall mechanics in anesthetized paralyzed humans. *J. Appl. Physiol.* 70:2602–2610, 1991.

[4] D'Angelo, E., E. Rocca, and J. Milic-Emili. A model analysis of the effects of different inspiratory flow patterns on inspiratory work during mechanical ventilation. *Eur. Respir. Monograph: Resp. Mech.* 12:279–295, 1999.

[5] Fredberg, J. J., and A. Hoenig. Mechanical response of the lungs at high frequencies. *J. Biomech. Eng.* 100:57–66, 1978.

[6] Ghazanshahi, S. D., and C. K. Khoo. Optimal application of high-frequency ventilation in infants: A theoretical study. *IEEE Trans. Biomed. Eng.* 40:788–795, 1993.

[7] Gillis, H. L., and K. R. Lutchen. Impact of heterogeneous bronchoconstriction on convective ventilation distributions among acini in humans. *Ann. Biomed. Eng.* 27:14–22, 1999.

[8] Gillis, H. L., and K. R. Lutchen. Airway remodeling in asthma amplifies heterogeneities in smooth muscle shortening causing hyper-responsiveness. *J. Appl. Physiol.* 86:2001–2012, 1999.

[9] Habib, R. H., R. B. Chalker, B. Suki, and A. C. Jackson. Airway geometry and wall mechanical properties estimated from subglottal input impedance in humans. *J. Appl. Physiol.* 77:441–451, 1994.

[10] Hantos, Z., B. Daroczy, B. Suki, S. Nagy, and J. J. Fredberg. Input impedance and peripheral inhomogeneity of dog lungs. *J. Appl. Physiol.* 72:168–178, 1992.

[11] Hickling, K. G. The pressure–volume curve is greatly modified by recruitment. A mathematical model of ARDS lung. *Am. J. Respir. Crit. Care Med.* 158:194–202, 1998.

[12] Horsfield, K., G. Dart, D. E. Olson, G. F. Filley, and G. Cumming. Models of the human bronchial tree. *J. Appl. Physiol.* 31:207–217, 1971.

[13] Horsfield, K., W. Kemp, and S. Phillips. An asymmetrical model of the airway of the dog lung. *J. Appl. Physiol.-Resp. Environ. Exercise Physiol.* 52:21–26, 1982.

[14] Lutchen, K. R., and K. D. Costa. Physiological interpretations based on lumped element models fit to respiratory impedance data: Use of forward-inverse modeling. *IEEE Trans. Biomed. Eng.* 37:1076–1085, 1990.

[15] Lutchen, K. R., K. Yang, D. W. Kaczka, and B. Suki. Optimal ventilation waveform for estimating low-frequency respiratory impedance. *J. Appl. Physiol.* 75:478–488, 1993.

[16] Lutchen, K. R., D. W. Kaczka, B. Suki, G. M. Barnas, P. Barbini, and G. Cevenini. Low-frequency respiratory mechanics using ventilator-driven oscillations. *J. Appl. Physiol.* 75:2549–2560, 1993.

[17] Lutchen, K. R., J. L. Greenstein, and B. Suki. How inhomogeneities and airway wall affect frequency dependence and separation of airway and tissue properties. *J. Appl. Physiol.* 80:1696–1707, 1996.

[18] Lutchen, K. R., and H. Gillis. Relationship between heterogeneous changes in airway morphometry and lung resistance and elastance. *J. Appl. Physiol.* 83:1192–1201, 1997.

[19] Marini, J. J., and P. S. Crooke. A general mathematical model for respiratory dynamics relevant to the clinical setting. *Am. Rev. Respir. Dis.* 147:14–24, 1993.

[20] Navajas, D., G. N. Maksym, and J. H. T. Bates. Dynamic viscoelastic nonlinearity of lung parenchymal tissue. *J. Appl. Physiol.* 79:348–356, 1995.

[21] Peslin, R., and J. J. Fredberg. Oscillation mechanics of the respiratory system. In: Handbook of Physiology. Mechanics of Breathing, edited by P. T. Macklem and J. Mead. Bethesda: American Physiological Society, 1986, pp. 145–177.

[22] Petak, F., M. J. Hayden, Z. Hantos, and P. D. Sly. Volume dependence of respiratory impedance in infants. *Am. J.*

Respir. Crit. Care Med. 156:1172–1177, 1997.
[23] Rossi, A., Polese, G., and J. Milic-Emili. Monitoring respiratory mechanics in ventilator-dependent patients. In: Principles and Practice of Intensive Care Monitoring, edited by M. J. Tobin. New York: McGraw-Hill, 1998, pp. 553–596.
[24] Schuessler, T. F., S. B. Gottfried, and J. H. T. Bates. A model of the spontaneous breathing patient: Applications to intrinsic PEEP and work of breathing. *J. Appl. Physiol.* 82:1694–1703, 1997.
[25] Sly, P. D., and J. H. T. Bates. Computer analysis of physical factors affecting the use of the interrupter technique in infants. *Pediatr. Pulmonol.* 4:219–224, 1988.
[26] Suki, B. Nonlinear phenomena in respiratory mechanical measurements. *J. Appl. Physiol.* 74:2574–2584, 1993.
[27] Suki, B., R. H. Habib, and A. C. Jackson. Wave propagation, input impedance, and wall mechanics of the calf trachea from 16 to 1600 Hz. *J. Appl. Physiol.* 75:2755–2766, 1993.
[28] Thorpe, C. W., and J. H. T. Bates. Effect of stochastic heterogeneity on lung impedance during acute bronchoconstriction: A model analysis. *J. Appl. Physiol.* 82:1616–1625, 1997.
[29] Vladimirescu, A. The Spice Book. New York: Wiley, 1994.